Materials Chemistry and Physics 260 (2021) 124183

Contents lists available at ScienceDirect

Materials Chemistry and Physics

journal homepage: www.elsevier.com/locate/matchemphys

Crystallization, structures and properties of biodegradable poly (butylene succinate-co-butylene terephthalate) with a symmetric composition

Cui Zheng [a], Guixiang Zhu [a], Ying Shi [b], Li-Zhi Liu [b,*], Minqiao Ren [a], Wei Zhang [a], Ling Han [a]

[a] SINOPEC Beijing Research Institute of Chemical Industry, Beijing, 100013, People's Republic of China
[b] Advanced Manufacturing Institute of Polymer Industry, Shenyang University of Chemical Technology, Shenyang, Liaoning Province, 110142, People's Republic of China

HIGHLIGHTS

- Studied structures at of biodegradable poly (butylene succinate-co-butylene terephthalate) with 50 mol% of BT.
- Achieved in-depth understanding of structure-property relationship about this material.
- Immature PBS crystals can form quickly under strain or very slowly (weeks) without strain, though not detectable by X-ray.
- Besides PBT crystals, PBS aggregates also contribute significantly to mechanical properties.
- This biodegradable copolymer potentially can have many industrial applications.

ARTICLE INFO

Keywords:
PBST
Biodegradable
Crystallization
Structure
Properties

ABSTRACT

The crystallization, crystalline structure, morphology and properties of poly (butylene succinate-co-butylene terephthalate) random copolymer (PBST) with 50 mol% of PBT, a very promising biodegradable polymer, was studied with a focus on understanding the structure property relationship. PBT spherulites are formed with an average diameter of ~11 μm, also implying a good crystal packing structure at lamellar level. The modulus and hardness of the copolymer are mainly contributed by the PBT crystals. It is known that no PBS crystal structure can be detected by X-ray diffraction; however, based on our FTIR and DSC studies, immature PBS crystals can be formed slowly (in days and months) at room temperature under no strain or quickly when stretched. These PBS aggregates contribute significantly to the mechanical properties of the copolymer, such as, mechanical strength, a good elongation to break and a permanent set at 80%. This biodegradable copolymer with a melting point (132 °C) close to HDPE, a modulus about 59 MPa, an elongation to break at 1300% and a shore D hardness of 42 can have many potential industrial applications.

1. Introduction

Poly(butylene succinate) (PBS) is a commercially available biodegradable aliphatic polyester, which is susceptible to microbial attack and being converted into carbon dioxide and water because of its vulnerable ester bonds presented in its main chains. [1–3], PBS potentially can have many applications [4] including food packaging, personal care, cosmetic, medical and automotive component, etc. [5] due to its good melt processability and chemical resistance. However, PBS also has its limitation for some applications, such as, a larger than 500% elongation is required; the elongation for PBS homopolymer is less than 300% [6,7]. One way to adjust its physical properties [8,9] is to blend PBS with a fraction of other polymer, such as poly(ethylene oxide) (PEO) [10], poly(lactic acid) (PLA) [11], poly(butylene adipate) (PBA) [12] and poly(butylene terephthalate) (PBT) [13], but the poor compatibility usually limits the applications, especially for its blends with rigid polymers [13,14]. A more effective way is copolymerization of PBS with other polymers, such as poly(ethylene succinate) (PES) [15], poly(propylene succinate) (PPS) [16], PBA [17] and PBT [18]. Among aromatic polyesters, PBT has excellent thermal and mechanical properties [19]. In addition, short butylene terephthalate segments with only 1 or 2 repeat unit can be biodegraded [20], which might be helpful for the biodegradability of the PBST random copolymer, as there may be a fraction of such short BT segments in PBST molecules.

* Corresponding author.
E-mail address: violetlj@yahoo.com (L.-Z. Liu).

https://doi.org/10.1016/j.matchemphys.2020.124183
Received 13 October 2020; Received in revised form 10 December 2020; Accepted 16 December 2020
Available online 18 December 2020

In fact, PBAT, the random copolymer of PBA and PBT with about 44 mol% PBT [21–24] has been a widely used biodegradable polymer in industry (such as, Ecoflex® by BASF Company), especially used for packaging films, compost bags and mulching films [25–29].

PBS has stronger crystalline ability (crystallizing earlier during a cooling process) and significantly higher melting point than PBA [30,31], the poly(butylene succinate-co-butylene terephthalate) copolymer or PBST could have some advantages over PBAT for some applications where a tougher material is required. PBST with the aromatic segment (terephthalate component) less than ~60 mol% can be bio-degradable [32,33]. As mentioned above, both the aliphatic ester and the single butylene terephthalate can be degraded through the metabolism of microorganisms [25], and the PBST with less BT content has faster degradation rate [18].

Some studies have been reported in literature on PBST random copolymer with 5–73 mol% of PBT [18,19,34,35].Very recently, efforts have been also made for synthesis of PBS-PBT multi-block copolymer based on the PBS and PBT blends with 31–87 mol% of PBT [36] and the synthesis of the branched copolymer with PBST backbone (about 50 mol % of PBT) and long PBST side chains [37]. However, in terms of the study of the structures and properties of PBST related copolymer, most reported studies were focused on the linear random PBST copolymers, which were first synthesized in 2000. Its biodegradability, physical properties, and processability change significantly with the copolymer composition. The glass transition temperature T_g of PBST increases monotonically with increasing the mole fraction of PBT in the copolymer [21,38]. The overall crystalline ability appears the weakest at a composition with ~30 mol% of BT, and the PBST material at this composition offers minimum strength due to minimum crystallinity and lowest melting point, but maximum elongation [21]. A very recent study also shows that a small fraction of poly(vinyl butyral) (PVB) added in the linear random PBST copolymer(regardless the composition) can play a very good nucleation role during the crystallization of the PBST [38]. The PBST with 30 mol% of PBT has been found to behave as a prominent memory thermoplastic material [39]. The PBST with 70 mol% of PBT (which is not biodegradable) may potentially have some advantages for fiber applications, and its structure changes during a uniaxial deformation process was also investigated [40–42]. When this PBST is stretched at high temperature (>100 °C), a fibrillary crystal structure could be formed [43,44]. The α-type PBT crystals can be switched to β-crystals during uniaxial stretching at room temperature for small strain (30–60%), but return to α-type when the load free [40].

In summary, poly (butylene succinate-co-butylene terephthalate) random copolymer (PBST) with 50 mol% of PBT can be a very promising biodegradable polymer, but its structure and property relationship are not well understood yet, especially the role of PBS segments on its performance. The literature studies on the linear random PBST copolymers are still very limited and the studies on structure and property were pretty much focused on the linear PBST random copolymer with 70 mol% of PBT with a potential fiber application, instead of biodegradable applications. In fact, the linear random PBST copolymer can also be a promising biodegradable polymer with many potential applications in different areas. As mentioned earlier, the commercial biodegradable PBAT with ~44 mol% of PBT has been widely used in many areas. The PBST with similar composition has been confirmed as a good biodegradable material [22] but is supposed to have some differences in properties compared with PBAT with similar composition, as PBS has a stronger crystalline ability than PBA. In addition, the PBST with ~50 mol% of PBT has the composition with a good balance of the biodegradability and the performance. Therefore, in depth understanding of biodegradable PBST is very much needed. In the present work, crystallization, structure, morphology, and properties of PBST with 50 mol% of PBT were studied. To have a good understanding of its crystallization behavior, selected PBST/PBS blend was also studied. In depth study of PBST with 50 mol% of PBT is helpful for a better understanding of the copolymer with other compositions which have not been well investigated in literature.

2. Experimental section

2.1. Materials

The PBST were prepared by melt polycondensation of 1,4-butanediol (BDO), purified terephthalate acid (PTA) and succinic acid (SA). Rare earth compound was used as the catalyst (see US patent US11312373). PTA, BDO and catalysts were added into a flask under a nitrogen atmosphere, and the mixture was then heated and stirred to a transparent solution, and then reacted at 180–200 °C. After most of the distilled water in the reaction had been removed, SA were added to the mixture and the temperature was raised to 200–220 °C. At the same time, the remaining water was removed. Vacuum degree was then increased gradually, and the reaction temperature was raised to 240–260 °C. Excess BDO was distilled in this period. Afterwards, high vacuum was applied. The final PBT mol% determined by ^{1}H nuclear magnetic resonance (^{1}H NMR) is 50%. The weight average molecular weight M_w of the synthesized material is 9.4×10^4, with the polydispersity $M_w/M_n = 1.64$ determined by gel permeation chromatography (GPC) at 25 °C with tetrahydrofuran (THF) as the fluent. The two homopolymers, PBS ($M_w = 12.0 \times 10^4$, $M_w/M_n = 1.70$) and PBT ($M_w = 11.5 \times 10^4$, $M_w/M_n = 1.66$), were also prepared by the same method, with the absent of PTA and SA, respectively. M-cresol was used for GPC characterization of PBS and PBT homopolymers.

2.2. Differential scanning calorimetry (DSC) study

The thermal behaviour of all the samples was characterized by a TA (USA) Q100 System under nitrogen gas flow. Sealed aluminium sample pans containing 3–6 mg of polymers were used in all the experiments. At the beginning of each experiment except noticed in the article, the samples were cooling rapidly to −60 °C and stay for 5 min. Then the samples underwent the heating-cooling-heating cycle in the range of −60 °C–250 °C at a rate of 10 °C/min. At each end of heating or cooling process, the sample pan was kept 5 min at the ending temperature (−60 °C or 250 °C).

2.3. Wide angle X-Ray diffraction (WAXD) study

The two-dimensional WAXD experiment was carried out on a Bruker (German) D8 DISCOVER 2D X-Ray diffractometer. The X-ray was generated using IμS micro Focus X-Ray source incorporating a 50W sealed-tube X-ray generator with Cu target. The wavelength is 0.154 nm (Cu Kα). The power of the generator used for measurement was 50 kV and 1 mA. The X-ray intensities were recorded on a VÅNTEC-500 2D detector system with a pixel size of 68 × 68 μm2. The spot size of the beam was 0.5 mm. The exposure time was 300 s LaB6 was used for broadening correction. The sample to detector distance was 20 cm. Crystal size along the normal direction of given crystal planes can be calculated by the Scherrer equation [45]:

$$D = \frac{K\gamma}{B\cos\theta} \quad (1)$$

where K is a shape factor (0.89), γ is the wavelength of X-ray (0.154 nm in our case), B is the Full Width at Half Maximum intensity (FWHM) of a diffraction peak in radians and θ is diffraction angle.

2.4. Small angle X-Ray scattering (SAXS) study

The SAXS measurements were conducted using Bruker (German) NANOSTAR U SAXS instrument. The X-ray source is IμS-type generator operated at 40 kV and 650 μA resulting in a wavelength (λ) of 0.154 nm (Cu Kα) in the experiment. The 3-pinhole collimation system provides a

precisely parallel X-ray beam with high intensity. The scattering intensity was detected by Hi Star area detector with1024 × 1024 pixels and 100 μm pixel size. The detector-to-sample distance is 1070 mm resulting enables a resolvable range of $0.09\ nm^{-1} \le q \le 2.0\ nm^{-1}$, where q is scattering vector ($q = 4\pi\sin(\theta/2)/\lambda$, where θ is the scattering angle). The SAXS data were calibrated for background scattering. Some X-ray experiments were conducted using synchrotron radiation with λ = 0.154 nm at Beamline 1W2A of Beijing Synchrotron Radiation Facility (Beijing, China). Mar165-CCD was used for data collection. All data were corrected for air background before any analysis. The average distance between neighbouring PBT crystals (L) can be determined from the position of a scattering peak, q_{max}, using Bragg's law [46].

$$L = 2\pi/q_{max} \quad (2)$$

2.5. Polarized optical microscopy (POM) study

The POM measurements were done using an Olympus (Japan) MODEL BX51TRF optical microscopy. The amplification ratio is 50 × .A thin film sample was firstly heated to melt (170 °C) between two glass sheets, and then cooled to room temperature for observation.

2.6. Light scattering (LS) study

The home-constructed configuration for LS consisted of a Compass 315M − 50 laser (Coherent, USA) with a wavelength = 532 nm, a polarizer and analyser (Daheng Optics, China), velum paper for image capture, and a PIX-1024BRXL camera (Princeton Instrument, USA) equipped with a G6 × 16–1.9 Macro-L camera lens (Spacecom, Japan). The polarizer and the analyser were set up for Hv configuration, i.e., the polarizing directions of the two lens is differed by 90°. The camera was positioned and focused to capture the scattering images on the velum paper. The sample-to-velum distance was changed according to the size of the scattering patterns. A thin film sample was firstly heated to melt (170 °C) between two glass sheets, and then cooled to room temperature for observation. The average radius spherulites, R, can be calculated with the equation [47] below:

$$R = \frac{4.09\lambda}{4\pi \sin\frac{\theta_m}{2}} \quad (3)$$

where λ is the wavelength of the laser (532 nm in our case) and θ_m is the scattering angle at scattering maximum.

2.7. Fourier transfer infrared (FTIR) study

Nicolet 6700 FTIR Spectrometer from Thermo Fisher Company with deuterated triglycine sulfate (DTGS) detector was used. FTIR spectra of PBS (thin film in KBr salt plate) were obtained at different temperatures using transmission mode with a resolution of 4 cm^{-1}. The attenuated total reflection mode (ATR) attachment was applied to the studies of PBT and PBST.

2.8. Hardness and mechanical testing

The hardness study was conducted by a Zwick/Roell (Germany) Digi Test 3115 instrument with a Shore D detector. The testing was done according to the standard GB/T 2411-2008/ISO 868:2003. Measurements of the mechanical properties of PBST, such as tensile strength, modulus, elongation at break and permanent set, were performed on a Shimadzu Corporation (Japan) AGS-X stress analysis instrument. The stretching speed 50 mm/min (250%/min) and a 1 kN load cell were used. According to GB/T 1040.2–2006, the sample size type of 5A, with gauge length 20.0 mm, broad 4.0 mm and thickness 2.0 mm, was taken.

3. Results and discussions

PBS and PBT homopolymers are incompatible, so their blends should show two individual glass transition temperatures (T_g) corresponding to the two homopolymers, respectively [13]. The PBST with the symmetric composition shows only a single T_g from the DSC heating curve shown in Fig. 1, indicating that material synthesized is a neat random copolymer with short PBS and PBT sequences. The observed T_g for the PBST with 50 mol% of PBT (PBST-50) is −15.8 °C, which is in between the glass transition temperatures of the two corresponding homopolymers (−31.0 °C for PBS and 40.5 °C for PBT), as shown in Fig. 1. The single T_g corresponds to the glass transition temperature of the amorphous region of the PBST consisting of short PBT and PBS sequences. The observed T_g for our PBST with 50 mol% of PBS is close to literature value for PBST with similar composition [18], and is 12 °C higher than the PBAT with 44 mol% of PBT segment [21], which is a commercial biodegradable material widely used for agriculture and packaging films [29]. The commercial PBAT film is relatively softer, due to the significantly lower T_g of PBA (−68 °C) [48] than PBS (−31.0 °C). The improved mechanical property of the biodegradable PBST over the PBAT can be important for some biodegradable applications.

3.1. Non-isothermal crystallization and thermal property of the copolymer

DSC Non-isothermal crystallization study (cooling at 10 °C/min from 250 °C) was carried out to understand the crystallization behavior of PBST-50, as shown in Fig. 2, together with the subsequent heating thermograms at 10 °C/min. The corresponding DSC thermograms of the two homopolymers are also shown in this figure for references. For the heating curves (Fig. 2b), both homopolymers show relatively narrow melting peaks. PBS presents a cold crystallization before its melting point T_m at 112.9 °C, which can be different to some degree depending on heating rate and annealing strategy [49,50]. The main melting point of PBT is around 210–225 °C. The double melting endotherm of PBT represents a melting/recrystallization/re-melting process for a faction of PBT crystals [51,52]. The fact that the melting point of the PBST-50 is higher than that of PBS suggests the crystals formed in the PBST correspond to the crystals formed by PBT segments. The T_m of the PBST is much lower than that of PBT homopolymer (132.1 °C vs. ~220 °C), which means the size of crystals in the copolymer is significantly smaller than that in the PBT homopolymer. The cooling thermogram (Fig. 2a) shows that both homopolymers show a sharp exothermic peak, and the crystallization temperature T_c is 69.1 °C for PBS and 187.9 °C for PBT,

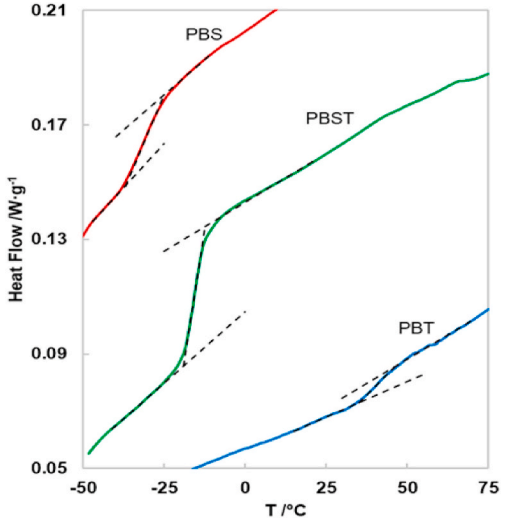

Fig. 1. DSC heating (10 °C/min) curves of PBST-50, PBS and PBT polymers.

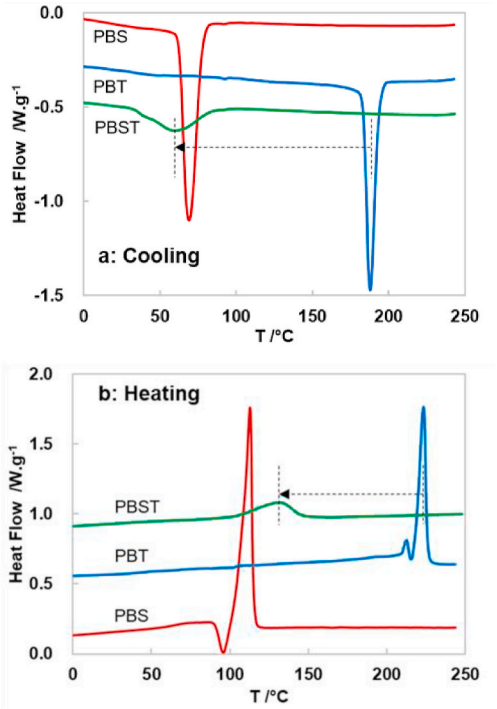

Fig. 2. DSC cooling (a) and subsequent heating curves (b) of PBST-50, and the corresponding PBS and PBT homopolymers (heating rate: 10 C/min).

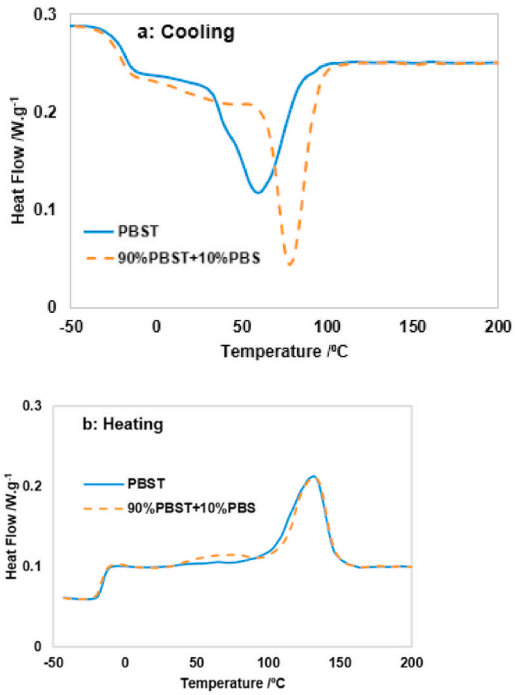

Fig. 3. The DSC cooling thermograms of the PBST with 50 mol% of PBT and its blend with 10 wt% of PBS homopolymer (a), as well as the subsequent heating thermograms (b).

respectively. The much lower T_c indicates that PBS has a much weaker crystalline ability than PBT, and it is consistent with the conclusion above that only PBT can crystallized in this random copolymer with a symmetric composition. The PBST-50 copolymer shows a very broad exothermic peak at 59.8 °C during the cooling process (Fig. 2a). As the melting peak of the copolymer has been attributed to PBT crystals, this crystallization peak during cooling is due to the crystallization of the PBT segments in the copolymer. The crystallization temperature, T_c, of the copolymer is also much lower than that in the PBT homopolymer (59.8 °C vs. 187.9 °C), indicating that the crystalline ability of PBT segments in the copolymer has been suppressed greatly. The much lower T_c and T_m of the PBST-50 than PBT homopolymer indicates that the segment length of PBT in the copolymer is very limited. However, the PBST-50 studied in this work has a significantly higher melting temperature (132.1 °C) than the widely used commercial PBAT (110 °C) [21], which suggests that the products made with this PBST also have a significantly better thermal stability than PBAT.

For the PBST with a symmetric composition of PBT and PBS, only PBT sequences can crystallize during the cooling, due to its much stronger crystalline ability. The PBS segments in the copolymer cannot crystallize during the cooling process at 10 °C/min, as indicated by the DSC 2nd melting thermogram. The crystallinity of PBT components in the PBST is 33% (calculated using the peak area at the 2nd heating curve, and the heat fusion 144.5 J/g for PBT perfect crystals [53]), meaning that the crystallinity of the copolymer is very low (~18%). In order to further confirm that the PBS sequences in the PBST copolymer with 50 mol% of PBT cannot crystallize during a cooling at 10 °C/min, crystallization of a blend of the PBST with 10 wt% of PBS homopolymer was also studied, as shown in Fig. 3. It is seen from Fig. 3a that the blend with 10% PBS homopolymer can crystallize at a significantly higher temperature than the neat PBST (77.8 °C vs. 59.8 °C). In fact, that the crystallization temperature of the blend is also significantly higher than the neat PBS homopolymer (69.1 °C). The nucleation and crystallization of the blend, observed at the significant higher temperature than both polymers, is presumably induced by the interface of the phase separation in this blend [54,55]. As can be seen from Fig. 3b, the main melting peak related to PBT crystals is pretty much the same for the neat copolymer and its blend with 10 wt% of PBS homopolymer, indicating the similar melting point and crystallinity for the crystals formed by PBT sequences. For the blend, a broad melting peak from 30 °C to 90 °C is also observed in Fig. 3b, which is related to crystals formed by PBS homopolymer or by both the homopolymer and PBS sequences in the copolymer. As the crystallinity of the neat PBS homopolymer, evaluated from the 2nd heating in Fig. 2b, is 58%, it is possible to evaluate the crystallinity of this lower melting peak to see if PBS sequences in the copolymer can co-crystallize with the PBS homopolymer. It is assumed that the PBS sequences in the copolymer cannot crystallize together with PBS homopolymer, and all the heat fusion related to the broad melting peak is contributed from the crystals formed by PBS homopolymer in the blend. If the evaluated PBS crystallinity of the blend is significantly larger than 58%, then the assumption is invalid, otherwise the assumption can be validated. Under this assumption, the evaluated crystallinity of for the broad melting within 30 °C–90 °C is only 34%, based on the heat fusion of 110.5 J/g for perfect PBS crystals [56]. This validates the assumption, which is, the PBS sequences in the copolymer cannot crystallize during the cooling process at 10 °C/min even with the presence of 10 wt% of PBS homopolymer.

In addition, the crystallinities of PBS and PBT homopolymers calculated from DSC data is 58% and 29%, respectively, and they are much larger than that of the copolymer. This may be one of the reasons why the copolymer has much larger elongation than the corresponding homopolymers (see Fig. 2).

3.2. *Crystalline structure and crystallinity of PBT segments in the copolymer*

The diffraction profiles of PBST-50, together with neat PBS and PBT, are shown in Fig. 4a. It can be seen from these profiles, that only α crystal form of the PBT [57,58] crystal is observed for the PBST-50 copolymer; no PBS diffraction peak is observed. The above observations are consistent with literature studies that only PBT crystals are formed for the PBST with >30 mol % of PBT [18]. In fact, it is also true that only

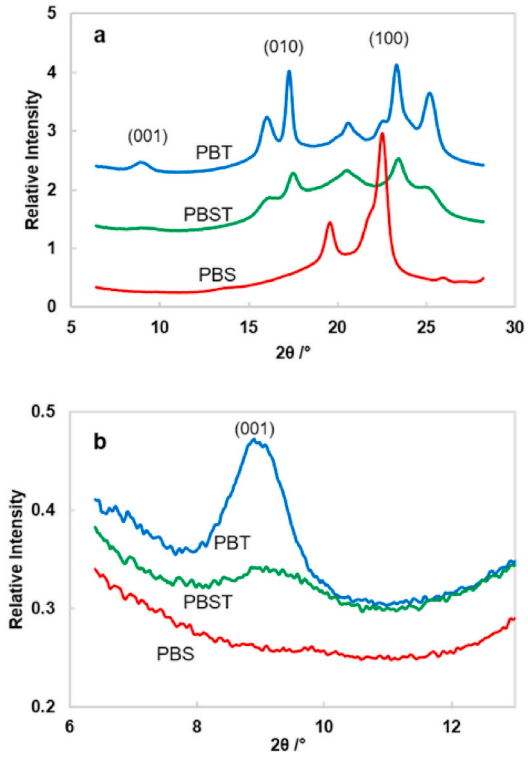

Fig. 4. WAXD profiles of the PBST with 50 mol% of PBT and the corresponding homopolymers (a) and a blow-up figure for (001) diffraction peak (b).

PBT crystals can be detected with WAXD for the widely used commercial PBAT with 44 mol% of PBT too [21]. On the other hand, it can be seen from Fig. 4a that the diffraction peaks of the PBST copolymer are broader than those from the neat PBT homopolymer, such as (001) peak (see Fig. 4b for a better view). This suggests that the PBT crystals formed in this copolymer are smaller than those in PBT homopolymer. Based on the peak widths, the average size of the PBT crystals can be estimated by Scherrer equation [45]. The estimated crystals size is 19 nm × 35 nm × 9.7 nm (in a, b, and c axis, respectively) for PBT homopolymer, and 9.3 nm × 14 nm × 3.4 nm for the copolymer. That is, the crystals in the copolymer are obviously smaller. It is known that lamellar stacks are formed during crystallization of PBT homopolymer [59,60]. As the crystal size calculated from (001) diffraction peak corresponds to the crystal size in polymer chain direction. That is, if lamellar structure still exists in the PBST-50 copolymer, the PBT lamellar crystals are supposed to be much thinner than those in PBT homopolymers. More discussions on this will be followed in later section together with results obtained with small angle laser light scattering.

For the PBST copolymer with 50 mol% BT crystallized under a cooling rate of 10 °C/min, the calculated crystallinity of PBT segments from the heating thermogram in Fig. 2, is about 33%, based on 144.5 J/g for 100% PBT crystallinity [53] and 56 wt% of PBT in the copolymer. The evaluated crystallinity for the copolymer is very similar to the crystallinity (36%) for the neat PBT homopolymer undergoing the same cooling process. That is, though the crystalline ability of PBT segments in the copolymer is significantly restricted, compared with neat PBT homopolymer, due to the copolymerization, the crystallinity of PBT sequences in the copolymer does not scarifies that much.

As the crystallinity of PBT sequences is only 33%, the rest of PBT sequences are supposed to be mixed at molecular level in the amorphous matrix with PBS sequences after the longer PBT sequences crystallize, showing a single glass transition near −16 °C. It is seen from the DSC cooling thermogram in Fig. 2 that PBT segments can crystallize at a very low temperature, such as, 40 °C with a peak crystallization temperature near 50 °C, during the cooling at 10 °C/min. This means that the 2nd crystallization of PBT segments can take place at room temperature for the copolymer. In fact, as shown in Fig. 5, the main melting peak at ~120 °C changed into a sharp peak with a slightly higher average melting point after the copolymer was kept at room temperature for 20 months, which is likely caused by PBT crystal thickening at room temperature. It is also interestingly noted that Fig. 5 also shows that a small melting peak around 160 °C, significantly higher than the main melting point, is present after the copolymer was kept at room temperature for six months and longer period, indicating some significant larger PBT crystals were formed at room temperature.

3.3. Crystallization of PBS segments

Crystallization of PBS homopolymer is relatively slow. In fact, crystallization of PBS homopolymer could not complete during a cooling at 10 °C/min and even slower cooling process [30], so cold crystallization is usually observed during the subsequent heating process (Fig. 2b). As shown in Fig. 2, the crystalline peak of PBS homopolymer is at 59.8 °C during the cooling from melt at 10 °C/min; the crystallize ability of PBS segments in the copolymer is supposed to be much weaker than the corresponding homopolymer. Though no PBS crystallization was detected during the DSC cooling 10 °C/min and subsequent heating (Fig. 2), the PBS sequences in the amorphous region may still be able to crystallize slowly at room temperature (above the T_g). In fact, the PBST-50 copolymer has a very low crystallinity (~18%) contributed by PBT sequences, and low T_g (−15.8 °C), so the copolymer with ~82% rubber phase is supposed to be a very soft material if PBS sequences do not crystallize at all. However, it is not and the measured Shore D hardness of the PBST-50 is about 42, which is very close to the hardness of the low-density polyethylene (which has a typical crystallinity of 40%) [61]. PBST-50 behaves more like a hard plastic rather than an elastomer. A more in-depth study of the structure in PBST-50 is needed and the PBS sequences may play a role for the hardness of the copolymer.

As shown in Fig. 2a, the PBT segments crystallize first due to stronger crystalline ability during a DSC cooling process, which makes the crystallization of PBS segments in the copolymer more difficult within the left-over space. However, considering the PBS content is about 50 mol%, which is significant, the PBS sequences could potentially be able to form crystal-like aggregates. The subsequent heating curve of the PBST copolymer (Fig. 2b) indicates that the PBS segments cannot crystallize at all during the cooling process at 10 °C/min. The very similar thermogram was also obtained from the subsequent heating, obtained after the sample was kept for 15 min at room temperature after the cooling, as shown in Fig. 5. However, as shown in Fig. 5, a distinct endothermic peak at ~55 °C appears after the PBST was kept at room temperature for one day. This melting peak becomes more pronounced with a longer annealing time at room temperature, as shown in Fig. 5 for 6 and 20

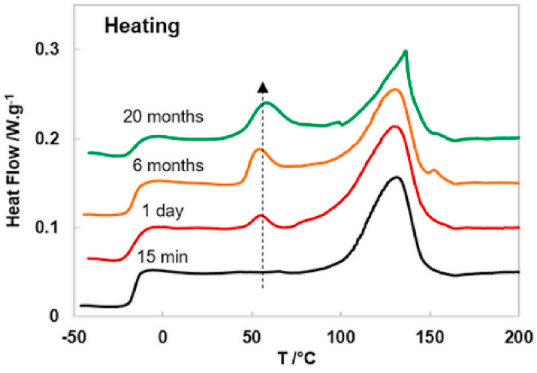

Fig. 5. DSC heating (10 °C/min) thermograms of the PBST-50 copolymer after the sample was crystallized by quenching from melt and kept at room temperature for 15 min, 1 day, 6 month and 20 months.

months. This melting at 55 °C is likely due to aggregates from PBS segments; WAXD and FTIR experiments were carried out in order to better understand the endothermic peak formed slowly at room temperature.

Two samples with different thermal history were prepared with the copolymer for the WAXD and FTIR study. The sample PBST-0 was crystallized by quenching from melt (170 °C for 5min) to 0 °C, FTIR data was collected immediately after the quench. The PBST-0 sample was kept at room temperature for one day (sample PBST-24hrs) and was used for FTIR data collection again. As both WAXD and FTIR experiment were finished within 20 min, the melting behaviour of samples PBST-0 and PBST-24hrs correspond to the DSC thermograms labelled "15 min" and "1 day", respectively in Fig. 5. As shown in Fig. 6a, no significant difference is observed from the WAXD profiles of the two samples, though the low melting peak at 55 °C is present for sample PBST-24hrs and it is absent for sample PBST-0. In other words, the WAXD study does not suggest that PBS sequences in the copolymer crystallizes slowly and contributed to the melting peak at 55 °C after kept at room temperature for one day (Fig. 5).

As the PBS sequences are supposed to be very short and it can be difficult to form large enough crystals to produce significant X-ray diffraction, especially considering the PBS crystallization occurs within the space left over after crystallization of PBT sequences. That is, fringe-micelles PBS crystals are still likely to be slowly formed at room temperature. As the chain conformations in crystal region, regardless big or small, and amorphous region are very different, and can be easily distinguished from FTIR study. As shown in Fig. 6b, the FTIR spectra of PBT homopolymer, crystallized PBS homopolymer, and amorphous PBS homopolymer are given for references. The IR spectra of the PBST-0 and PBST-24hrs, collected immediately after quenched from melt and one day after, respectively, are also shown in the figure. The unique wave numbers, where IR peaks from PBS crystal phase are present but absent from PBT crystal phase, are marked by the vertical dash lines in Fig. 6 (b). By comparing the spectra of the PBST-24hrs and PBST-0, it can be seen that a few IR peaks related to PBS crystal become more pronounced after the copolymer was kept at room temperature for one day. This implies that the melting peak at 55 °C in Fig. 5 is contributed by small PBS crystals, likely fringe-micelles crystals.

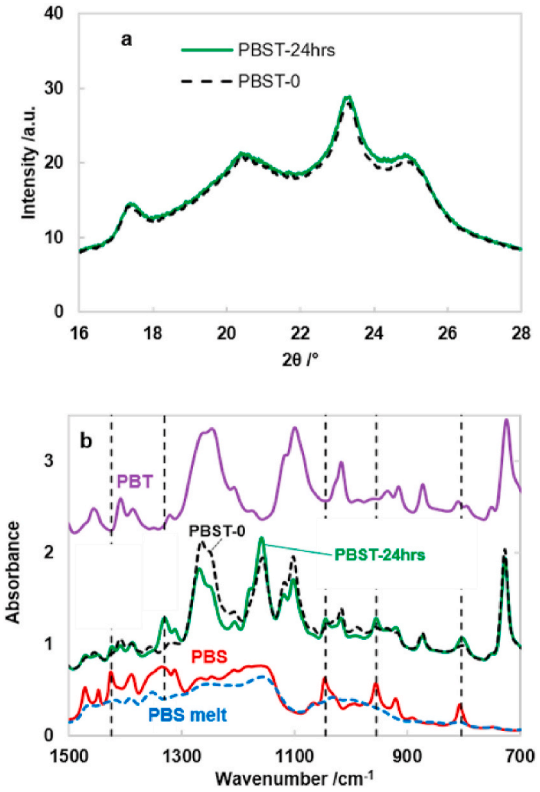

Fig. 6. (a) WAXD profiles of the PBST-50 copolymer collected immediately after quenched from melt (PBST-0) and collected one day later (PBST-24hrs). (b) FTIR spectra of PBT homopolymer (top solid, room temperature), crystallized PBS homopolymer (25 °C, solid line at bottom), and amorphous PBS homopolymer collected in melt state (180 °C, dash line at bottom), as well as the IR spectra of PBST-0 (middle dash line) and PBST-24hrs (middle solid line). The vertical dash lines mark the wave numbers for the unique IR peaks of crystallized PBS where no IR peaks from PBT crystals are present.

3.4. Crystal packing structure and morphology

The SAXS scattering curves of PBST-50 and the two corresponding homopolymers were shown in Fig. 7. The inter-crystal distance or long period for the polymers can be determined from the scattering maxima. The long period for PBS and PBT homopolymers is 8.0 and 11.4 nm, respectively. The inter-crystal distance for the PBST-50 copolymer is appreciably larger (13.1 nm) than the homopolymers. The larger long period for the PBST-50 than PBT homopolymer indicates a larger separation distance of crystals in the copolymer than in the homopolymers. In fact, spherulites can also be formed in the PBST-50 copolymer, as shown in Fig. 8a for the photo obtained from a polarized optical microscopy and the image from laser light scattering in Fig. 8b. The calculated average radius of the spherulites is 5.7 μm. It is interesting that the copolymer can still form well defined PBT spherulites which are impinged together, considering that the copolymer has a very low PBT crystallinity (~18%). Typically, a spherulite consists of many fibrillar crystals made of alternating crystal and amorphous lamellar stacks. With the assumption that the bulk crystallinity of the materials (~18% for PBST-50 and 36% for PBT homopolymer) is the same as the one-dimensional crystallinity, the thickness of the crystal lamella can be estimated based on the long periods obtained. The estimated average crystal lamellar thickness is 2.4 and 4.1 nm for PBST-50 copolymer and PBT homopolymer, respectively. The significant thinner thickness of PBT lamellae in the PBST copolymer than that of the neat PBT homopolymer are consistent with the significantly lower melting temperature of the copolymer (132 °C) than PBT homopolymer (~220 °C).

The mechanical property of PBST with different compositions (11–73 mol % of PBT), such as, yield strength and elongation at break, have been reported in literature [18]. In this section, the discussion is focused on the structure-property relationship of the PBST with 50 mol% of PBT for a uniaxial stretching process. The tensile property of the PBST is very different from both homopolymers. The uniaxial stretching study was carried out for this copolymer. The engineering stress–strain curve is shown in Fig. 9 together with the corresponding curves for the two homopolymers. As can be seen from this figure, the PBST copolymer is much more ductile than both homopolymers. The Young's modulus of

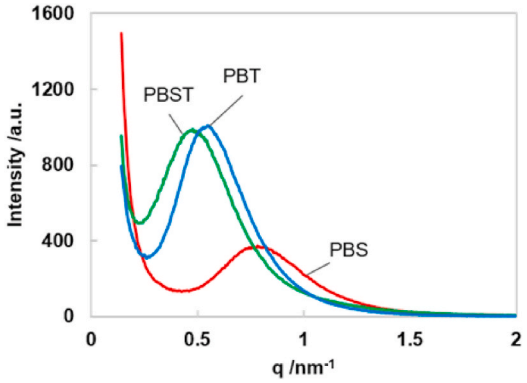

Fig. 7. SAXS profiles of the PBST-50 and the corresponding PBS and PBT homopolymers.

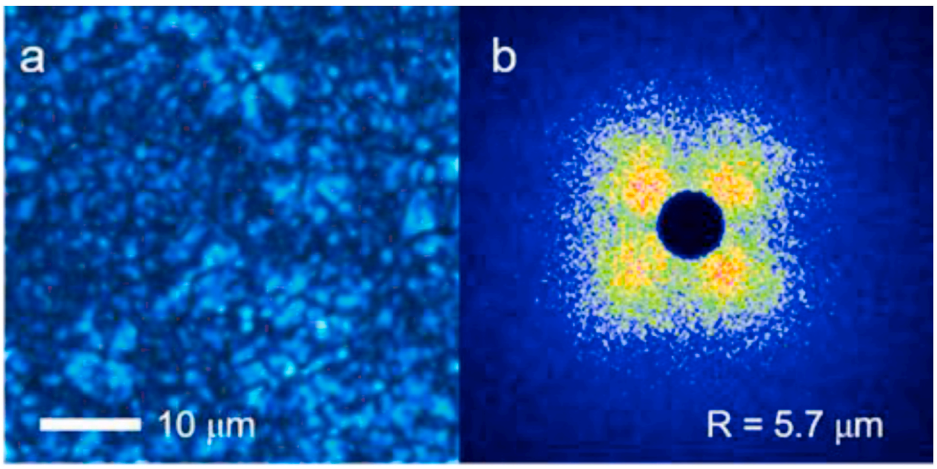

Fig. 8. Polarized optical image (a) and light scattering pattern of PBST-50 (b). Structure-property relationship studied with a uniaxial stretching process.

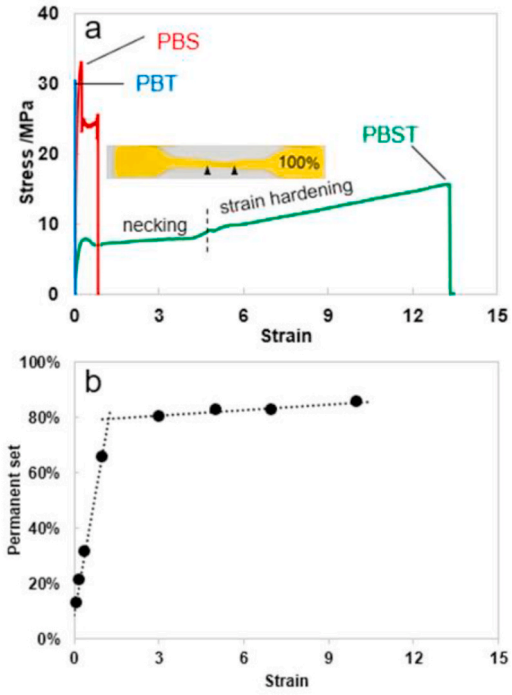

Fig. 9. (a) The engineering stress-strain curves of PBST-50 copolymer and the corresponding, PBS and PBT homopolymers obtained from a uniaxial stretching process at a speed of 50 mm/min with an initial length of 20 mm. The inset picture shows the necking of the copolymer at a strain of 1. (b) the permanent set of PBST-50 at different strains.

the copolymer is 59 MPa, evaluated based on the initial elastic region of the stress-strain curve, and the stress at the yield point with a strain of 0.4 is 8 MPa. Both the modulus and the yield strength of the copolymer are significantly lower than the two homopolymers, as shown in Fig. 9. But the elongation to break is dramatically larger than both homopolymers. The stress increases very slowly with increases in strain due to the long necking process (up to a strain of 4), and then increases sharply for the strain hardening process, until the elongation to break at a strain of ~13. The permanent sets of the copolymer stretched to different strains are shown in Fig. 9b. It can be seen from this figure that the permanent set is small with limited deformation, but for strain larger than 1.3, the permanent set is as high as 80%, as shown in Fig. 9b. That is, the material can have a very large elongation to break (1300%), but it is not an elastomer. That is, the biodegradable PBST with 50 mol% of PBT has a significantly higher Young's modulus (59 MPa), yield strength (8 MPa) and elongation to break ratio (1300%) than the widely used commercial PBAT with 44 mol % of PBT with Young's modulus of 30 MPa, yield strength of 6 MPa and elongation to break ratio about 1000% [62].

The structure change during the uniaxial stretching process of the copolymer is also studied with WAXD and SAXS. As the necking process goes all the way to a strain near 4, the sample is not uniform due to the existence of necking and non-necking regions. The structure data within the necking is not covered in this section. The selected 2D WAXD and 2D SAXS images for the uniaxial stretching process of the copolymer are shown in Fig. 10. It can be seen from WAXD patterns in Fig. 10 that for an elongation of 40% near yielding point, no obvious crystal orientation is observed. After the necking process is finished, such as, at an elongation at 500%, the PBT crystals in the PBST copolymer are very oriented, as shown in Fig. 10. Further increase in elongation to 1300%, a very oriented diffraction pattern like typical fiber diffraction is observed (Fig. 10). The SAXS study on the PBT crystal packing also shows that no obvious crystal orientation is observed before yield point, but strong PBT crystal orientation is observed after the yield of the PBST copolymer, as shown in Fig. 10. It is also noticed that no diffraction peaks associated with PBS crystals are observed during the stretching process. In fact, for the PBST copolymer with more PBS content, such as, 68 mol %, the PBS diffraction peaks can be identified [19] and for the PBST copolymer with 65 mol% of PBS, PBS diffraction can also be observed if stretched [39].

The SAXS profiles in stretching direction are shown in Fig. 11 (a), and it can be seen from this figure that the scattering maxima moves to a much larger q after the necking is finished for a strain range over 4, indicating that old PBT crystals are destroyed and new PBT crystals are formed with a significant smaller long period. The average distance for the neighbouring PBT crystals (long period) at different strain can be evaluated from the peak position of a scattering profile and is shown in Fig. 11b (right).

Crystal orientation are evaluated with (110) diffraction based the WAXD patterns in Fig. 10 and is also shown in Fig. 11 (b). It can be seen from Fig. 11 that after the necking process is over, the crystal orientation increases very significantly, and keeps increasing with further increase in strain.

The long period, however, shows a big drop after the necking process; it starts about 14 nm before the stretching and decreases to about 8 nm at a strain of 5. Considering that at strain of 13 (elongation to break) the crystals still have a long period slightly larger than 8 nm, and that the original crystals packing after fragmentation are not supposed to survive an elongation of 1300%, the crystals with a long period around 8 nm, represented in Fig. 11 (b) with strain larger than 5, can be attributed to

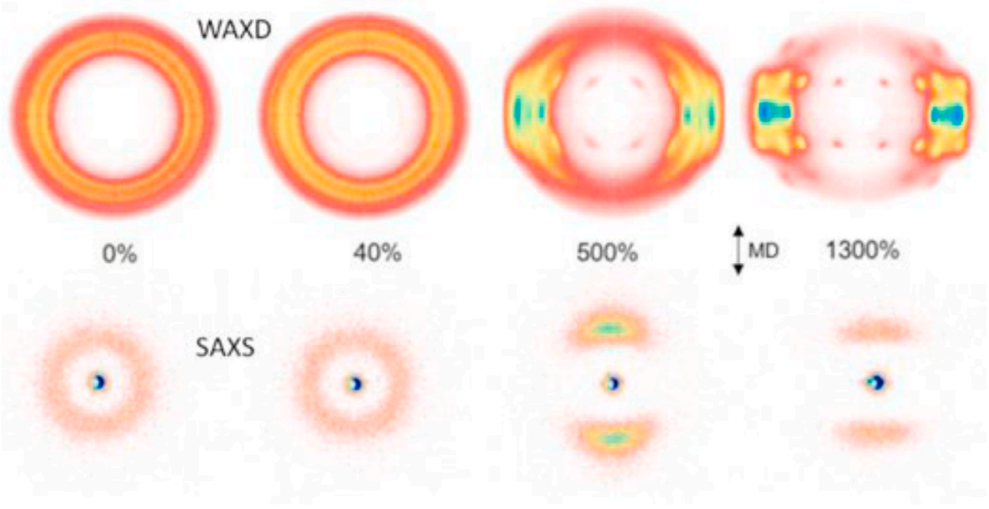

Fig. 10. Selected 2D WAXD and 2D SAXS of PBST-50 copolymer stretched to different elongation with the arrow indicating the stretching direction.

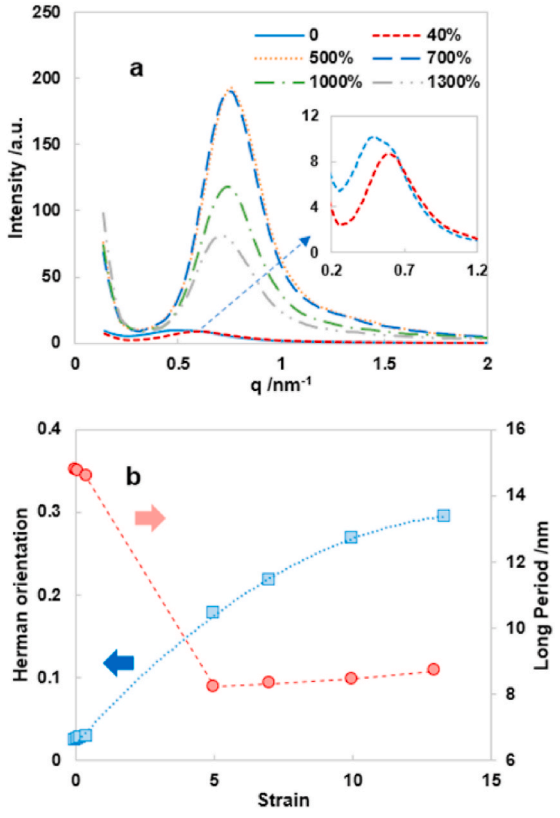

Fig. 11. a). SAXS profiles of PBST-50 in stretching direction (the SAXS profiles at strain of 0 and 0.4 can be better seen from the inset figure); b). the long period of PBT crystals in the stretched PBST-50 (right), determined from the SAXS profiles, and the corresponding Herman orientation factor (left), determined from (110) diffraction based the WAXD patterns in Fig. 10.

orientation-induced new crystals at large strain over 5. The slight increase in long period with strain at the strain range larger than 5 is likely due to the more oriented amorphous in stretching direction.

As discussed in previous section about Fig. 5, except the melting peak of PBT crystals at 113 °C, a weak endothermic peak at ~55 °C appears after the copolymer was kept at room temperature for one day (also shown in Fig. 12 together with deformed samples), due to the slow formation of PBS crystals, confirmed by the FTIR experiment in this

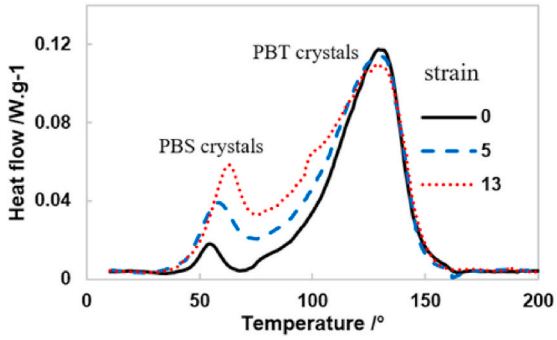

Fig. 12. DSC heating curves of the PBST copolymer after uniaxially stretched with a stain of 0, 5 and 13, respectively (data collected 2–3 h after the stretching), together with the DSC scan of the non-deformed copolymer, which was kept at room temperature for one day after cooling down from melt.

work. This PBS melting peak becomes more pronounced with a longer annealing time at room temperature, such as, 6 months. However, the uniaxially stretching can speed up the crystallization of PBS sequences, a much larger melting peak near 55 °C is observed after the sample is stretched for 500% and 1300%, respectively, as shown in Fig. 12. The PBS crystallization is supposed to happen during the stretching process, though the DSC data was collected 2–3 h later. Furthermore, it is seen from Fig. 12 that a broad melting is also observed between 60 and 110 °C for the stretched samples, and the broad melting increases with increase in strain. Fig. 12 shows that the stretched PBST has a significantly higher crystallinity than the un-stretched one, and the crystallinity increases with increase in strain. The broad melting between 60 and 110 °C is mainly contributed by PBS crystals, but it cannot be ruled out that the melting can be partially contributed by small PBT crystals induced during the stretching process. The PBS sequences are very likely to form small and immature fringe-micellar crystals, so it is not detectable with X-ray diffraction. In contrast, for the commercial PBAT with 44 mol% of PBT, the crystallization of PBA segments can only occur in ultra-high strain region in case of the PBAT fiber [22].

With the above crystallization and structure studies on the copolymer, the mechanical properties can be better understood. The PBT sequences has about 18% of crystallinity and the PBS sequences crystalize can only slowly (days and months) at room temperature in case of no deformation with very low crystallinity. The soft matrix (a low T_g, −15.8 °C, for the amorphous phase of this copolymer) enables the formation of the spherulitic morphology driven by crystallization of PBT

sequences. The modulus of 59 MPa and hardness of 42 (shore D), close to low-density polyethylene, should be mainly contributed by the spherulitic morphology with PBT crystals. The PBS sequences can crystallize quickly when stretched, which is consistent with the high permanent set (around 80%) for this copolymer. The quick PBS crystallization under strain should contribute significantly to the mechanical properties of the copolymer, like mechanical strength and elongation to break. The very large elongation of the copolymer (1300%) shown in Fig. 2 can be contributed by low crystallinity of PBT sequences and stretching induced fringe-micellar PBS crystals.

4. Conclusions

The crystalline ability of both components of the biodegradable poly (butylene succinate-co-butylene terephthalate) random copolymer (PBST) with a 50/50 mol composition is greatly restricted in the copolymer, especially for PBS segments. The melting temperature of PBT crystals formed in the PBST is around 132 °C. No PBS crystallization can be detected during the DSC cooling and subsequent heating processes. No PBS crystallinity can be detected by X-ray diffraction as it is difficult to form three dimensional ordered PBS crystals within the left-over space after PBT crystallization; this is also true for stretched sample and for un-deformed sample kept at room temperature for months. The formation of PBT spherulites with an average diameter of ~11 μm also implies a good crystal packing at lamellar level. The modulus of 59 MPa and hardness of 42 (shore D) of the copolymer, close to low-density polyethylene, should be mainly contributed by the spherulitic morphology with PBT crystals.

However, the PBS sequences can crystallize quickly when stretched and are able to crystalize slowly (days and months) at room temperature for non-deformed sample, confirmed by DSC and FTIR studies. These studies indicate that only very immature PBS crystals can be formed slowly at room temperature or quickly by stretching the material. Moreover, crystallizing quickly under strain for PBS sequences should contribute significantly to the mechanical properties of the copolymer, like mechanical strength and elongation to break and a permanent set around 80%.

With the in-depth understanding of the crystallization behaviour of PBS sequences, the mechanical properties of the PBST can be better understood. This biodegradable copolymer with a melting point about 132 °C (close to HDPE), the modulus of 59 MPa, an elongation to break about 1300% and a shore D hardness of 42 can have many potential industrial applications such as some special films and bags.

CRediT authorship contribution statement

Cui Zheng: Data curation, Formal analysis, Writing - original draft, Most of the experiments, Data Analysis, draft Writing. **Guixiang Zhu:** Synthesis. **Ying Shi:** Writing - review & editing. **Li-Zhi Liu:** Conceptualization, Supervision. **Minqiao Ren:** DSC, WAXD experiments. **Wei Zhang:** Synthesis support. **Ling Han:** Synthesis support.

Declaration of competing interest

The authors declare that they have no known competing financial interests or personal relationships that could have appeared to influence the work reported in this paper.

Acknowledgements

The authors would also like to thank Dr. Xuanbo Liu for his help with the DSC measurements, Dr. Juan Li and Dr. Bin Wang for their help with the FTIR measurements, and Mr. Yi Ren for his help with the tensile measurements. This work was partially supported by Liaoning Pandeng Scholar program. Part of the SAXS experiment was done with synchrotron radiation at beamline 1W2A of the Beijing Synchrotron Radiation Facility (BSRF).

Appendix A. Supplementary data

Supplementary data to this article can be found online at https://doi.org/10.1016/j.matchemphys.2020.124183.

References

[1] M. Vert, S.M. Li, G. Spenlehauer, et al., J. Mater. Sci. Mater. Med. 3 (1992) 432–446.
[2] M. Mochizuki, M. Hirami, Polym. Adv. Technol. 98 (1997) 3437–3447.
[3] A.A. Shah, S. Kato, N. Shintani, et al., Appl. Microbiol. Biotechnol. 98 (2014) 3437–3447.
[4] W. Zhang, J. Ji, J. Zhao, et al., N. Chem. Mater. 38 (2010) 1–5.
[5] A. Soroudi, I. Jakubowicz, Eur. Polym. J. 49 (2013) 2839–2858.
[6] G.Q. Chen, M.K. Patel, Chem. Rev. 112 (2012) 2082–2099.
[7] S. Weerasunthorn, P. Potiyaraj, Adv. Mater. Res. 1025–1026 (2014) 215–220.
[8] H.C. Ki, O.O. Park, Polymer 42 (2001) 1849–1861.
[9] M. Ngouajio, R. Auras, R.T. Fernandez, et al., HortTechnology 18 (2008) 605–610.
[10] Y. He, B. Zhu, W. Kai, et al., Macromolecules 37 (2004) 3337–3345.
[11] A. Bhatia, R.K. Gupta, S.N. Bhattacharya, et al., Korea-Australia rheology j 19 (2007) 125–131.
[12] H.J. Wang, H.P. Feng, X.C. Wang, et al., Chin. J. Polym. Sci. 32 (2014) 488–496.
[13] Y.J. Kim, O.O. Park, J. Appl. Polym. Sci. 72 (1999) 945–951.
[14] A.C. Quental, F.P.D. Carvalho, M.L. Rezende, et al., J. Polym. Environ. 18 (2010) 308–317.
[15] Z. Gan, H. Abe, Y. Doi, Biomacromolecules 2 (2001) 313–321.
[16] Y. Xu, J. Xu, D. Liu, et al., J. Appl. Polym 109 (2010) 1881–1889.
[17] G.X. Chen, J.S. Yoon, J. Polym.B: Polym. Phys 43 (2005) 478–487.
[18] M. Nagata, H. Goto, W. Sakai, N. Tsutsumi, Polymer 41 (2000) 4373–4376.
[19] F. Li, X. Xu, Q. Hao, et al., J. Polym. Sci. B Polym. Phys. 44 (2010) 1635–1644.
[20] U. Witt, R.-J. Müller, W.D. Deckwer, J. Environ. Polym. Degrad. 5 (1997) 81–89.
[21] K. Kuwabara, Z. Gan, T. Nakamura, et al., Biomacromolecules 3 (2002) 390–396.
[22] X.Q. Shi, H. Ito, T. Kikutani, Polymer 46 (2005) 11442–11450.
[23] E. Cranston, J. Kawada, S. Raymond, et al., Biomacromolecules 4 (2003) 995–999.
[24] K. Kuwabara, M. Yamamoto, H. Abe, et al., Polym. Degrad. Stabil. 83 (2004) 289–300.
[25] U. Witt, M. Yamamoto, U. Seeliger, et al., Angew. Chem. Int. Ed. 38 (1999) 1438–1442.
[26] http://www.plasticsportal.net/wa/plasticsEU/portal/show/content/products/biodegradable_plastics/biodegradable_polymers.
[27] U. Witt, T. Einig, M. Yamamoto, et al., Chemosphere 44 (2001) 289–299.
[28] X. Wu, C. Fu, Z. Tan, et al., J. Appl. Polym 137 (2020) 48577.
[29] A. Morro, F. Catalina, E. Sanchez-Leon, et al., J. Polym. Environ. 27 (2019) 352–363.
[30] E.S. Yoo, S.S. Im, J. Polym.B: Polym. Phys 37 (2015) 1357–1366.
[31] Z. Gan, K. Kuwabara, H. Abe, et al., Biomacromolecules 5 (2004) 371–378.
[32] N. Honda, I. Taniguchi, M. Miyamoto, et al., Macromolecular Bioence 3 (2003) 189–197.
[33] A.A. Shah, T. Eguchi, D. Mayumi, et al., Polym. Degrad. Stabil. 98 (2013) 609–618.
[34] L. Ren, Y. Wang, J. Ge, et al., Macromol. Chem. Phys. 216 (2015) 636–640.
[35] F. Li, X. Xu, J. Yu, et al., Polym. Degrad. Stabil. 92 (2007) 1053–1060.
[36] C.W. Lee, M. Akashi, Y. Kimura, et al., Macromol. Res. 25 (2017) 1–9.
[37] J. Lu, L. Wu, B.G. Li, J. Appl. Polym. Sci. 134 (2017) 44544.
[38] B. Yang, S. Zhu, Y. Luo, et al., J. Polym.B .: Polym. Phys 55 (2017) 658–672.
[39] Y. Shi, C. Zheng, G. Zhu, et al., React. Funct. Polym. 154 (2020) 104680.
[40] J. Zhang, X. Wang, F. Li, et al., Fibers Polym. 13 (2012) 1233–1238.
[41] F. Li, S. Luo, J. Zhang, J. Therm. Anal. Calorim. 113 (2013) 915–921.
[42] Z. Wei, Z. Pan, F. Li, et al., RSC Adv. 8 (2018) 1378–1384.
[43] Z. Wei, R. Lun, X. Lou, et al., RSC Adv. 4 (2014) 64625–64633.
[44] Z. Wei, J. Lin, F. Tian, et al., J. Polym.B: Polym. Phys 53 (2015) 640–649.
[45] U. Holzwarth, N. Gibson, Nat. Nanotechnol. 6 (2011) 534.
[46] R.J. Roe, X-Ray Diffraction by Polymers, John Wiley & Sons, Inc., 2015.
[47] R.J. Samuels, Structured Polymer Properties, Wiley Interscience, New York, 1974, p. 82.
[48] Z. Gan, K. Kuwabara, M. Yamamoto, et al., Polym. Degrad. Stabil. 83 (2004) 289–300.
[49] T. Yokohara, K. Okamoto, M. Yamaguchi, J. Appl. Polym 117 (2010) 2226–2232.
[50] X. Wang, J. Zhou, L. Li, Eur. Polym. J. 43 (2007) 3163–3170.
[51] M. Li, Y.G. Jeong, J. Appl. Polym 125 (2012) E532–E540.
[52] M.E. Nichols, R.E. Robertson, J. Polym. Sci. B Polym. Phys. 30 (1992) 755–768.
[53] M. Nagata, T. Kiyotsukuri, S. Takeuchi, et al., Polym. Int. 42 (1997) 33–38.
[54] Y. Niu, L. Yang, H. Wang, et al., Macromolecules 42 (2009) 7623–7626.
[55] W. Shao, Y. Zhang, Z. Wang, et al., Ind. Eng. Chem. Res. 51 (2012) 15953–15961.
[56] S. Fakirov, T. Gogeva, Makromol. Chem. 191 (1990) 615–624.
[57] M. Yokouchi, Y. Sakakibara, Y. Chatani, et al., Macromolecules 9 (1976) 266–273.
[58] T. Ni, G.S. Huang, J. Zheng, et al., Polym. J. 42 (2010) 357–362.
[59] J. Runt, D.M. Miley, X. Zhang, et al., Macromolecules 25 (1992) 1772–1780.
[60] M.L.D. Lorenzo, M.C. Righetti, Polym. Bull. 53 (2004) 53–62.
[61] E.M. Kampouris, A.G. Andreopoulos, Eur. Polym. J. 25 (1989) 321–324.
[62] J. Zhou, Y. Zheng, G. Shan, et al., Macromolecules 52 (2019) 1334–1347.